Wear 514-515 (2023) 204564

Contents lists available at ScienceDirect

Wear

journal homepage: www.elsevier.com/locate/wear

Research on friction performance and wear rate prediction of high-speed train brake pads

Jiawei Chen [a], Chunyu Yu [a,*], Qi Cheng [a], Yuanlin Guan [a], Qinghai Zhang [a], Weipu Li [a], Fuhao Ouyang [a], Zhenning Wang [b]

[a] *School of Mechanical and Automotive Engineering, Qingdao University of Technology, Qingdao, Shandong, 266520, China*

[b] *Shandong Baiderui Rail Traffic Technology Co., Ltd, Qingdao, Shandong, 266432, China*

A R T I C L E I N F O

Keywords:
Cu-based PM brake pad
Friction performance
Wear rate prediction
Temperature
Braking distance
ASO-BP

A B S T R A C T

As we know, the wear of high-speed trains cannot be avoided, otherwise it cannot brake and stop. But its operating environments are complex and changeable, leading to insufficient research on friction performance of copper (Cu)-based powder metallurgy (PM) brake pads and difficult prediction of the wear rate. Therefore, we explore the variation trend of the friction performance of the brake pad with different multi-factors coupling braking conditions, and predict the wear rate of Cu-based PM brake pad based on Atom Search Optimization-Back Propagation (ASO-BP) neural network. The Cu-based PM brake pad regarded as the research object whose friction coefficient, friction temperature, braking distance, wear rate, and change mechanism are discussed with multi-factors coupling braking conditions, and wear rate is predicted based on ASO-BP neural network that can obtained by optimizing the weights and thresholds of the Back Propagation (BP) neural network with Atom Search Optimization (ASO) method. The results show that braking speed and braking pressure are main contributors to braking ability, the average coefficient of friction of the Cu-based PM brake pads varied nearly between 0.35 and 0.45 with different braking conditions, the maximum of temperature, braking distance, braking time and the wear rate of the brake pad are 473 °C, 3506 m, 138s and 0.14 cm^3/MJ, respectively. And the prediction accuracy of brake pad wear rate based on ASO-BP neural network can reach 97.3%.

1. Introduction

As an important component of the high-speed train braking system, the brake pad plays a decisive role in the braking of the high-speed train [1]. In order to ensure the safe operation of trains, the braking performance of trains becomes more important with the development of high-speed railways and the improvement of train speed. As the key component of the braking system, it is significant to explore the friction performance and wear rate of the brake pad.

The braking ability of high-speed trains is closely related to the materials of the brake pad. In China, the brake pad can be mainly divided into powder metallurgy (PM) brake pads and synthetic brake pads according to different manufacturing processes. PM brake pads are prepared by sintering and pressing processes at high temperature, while synthetic brake pads are prepared by melting and casting processes. However, both the braking power and braking stability of synthetic brake pads are poor with the increase of temperature and thermal load [2,3]. Compared with the synthetic brake pad, the PM brake pad has good wear resistance, good thermal conductivity, resistance bond and porosity besides excellent braking power and braking stability [4,5]. Therefore, PM brake pads have concentrated more and more attentions of researchers in high-speed train field.

In recent years, most of the research in this field is focused on Cu-based PM brake pads. There are some researches studying the effect of Al_2O_3, TiC, carbon fiber, and other materials on the performance of Cu-based PM brake pads with different braking speeds and braking pressures [6–9]. There are also some scholars studying the manufacturing process [10,11], shape [12,13], vibration and noise [14,15], friction and wear [16–18] on the performance of the brake pad. Although the above research has made some achievements, it is insufficient research on the friction performance of high-speed train brake pads with multi-factor coupling conditions.

Some studies obtain the wear state images of brake pad and use mathematical methods to predict its wear. For example, Li [19] used the

* Corresponding author.
E-mail address: yuchunyu@qut.edu.cn (C. Yu).

https://doi.org/10.1016/j.wear.2022.204564
Received 10 July 2022; Received in revised form 27 October 2022; Accepted 18 November 2022
Available online 19 November 2022

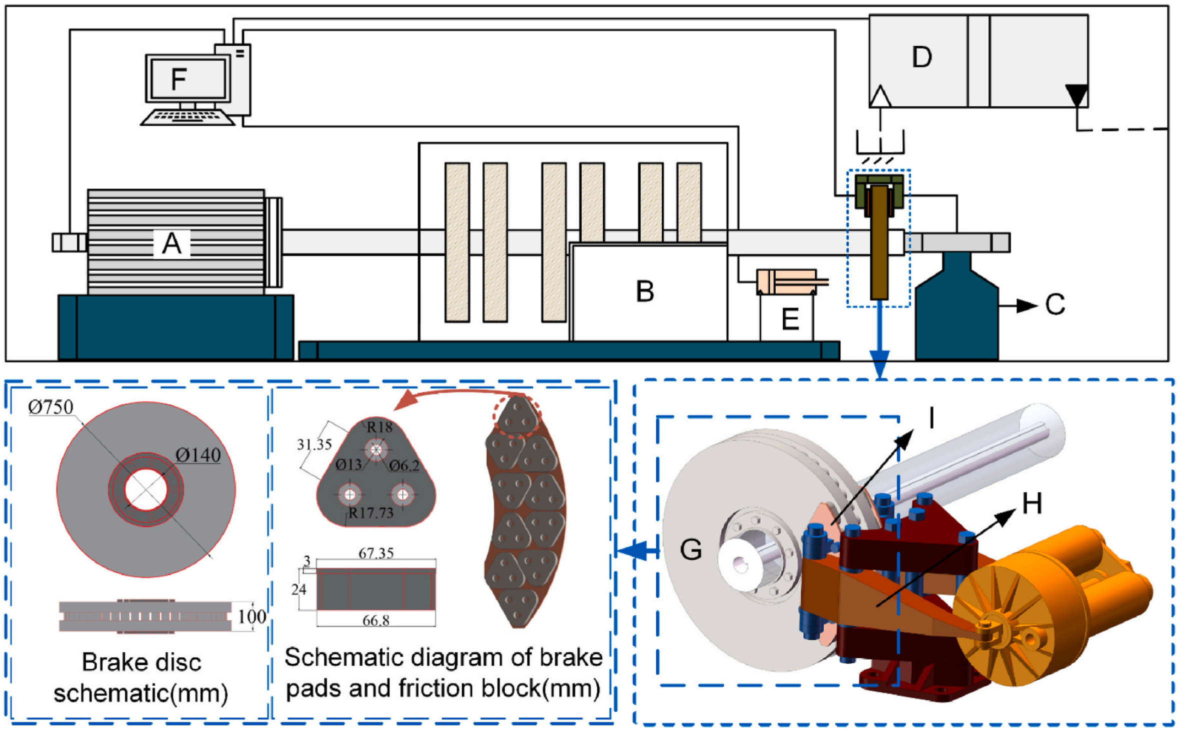

Fig. 1. Schematic diagram of the experimental platform and brake disc and brake pad.

support vector machine (SVM) to identify the edge features of brake pad and used the least squares support vector machine (LSSVM) algorithm to predict the wear of the brake pad, which was more accurate than the traditional neural network algorithm. Kumar et al. [20] used artificial neural network (ANN) to predict the wear and friction coefficient of brake pad, compared with the actual test data, and the prediction errors were less than 3% and 4% respectively. Wang et al. [21] predicted the wear of brake shoe based on a deep belief network (DBN), they found that the prediction accuracy increased significantly with increasing mileage of train. Xu et al. [22] proposed a model combining multi-scale convolution (CNN) and convolutional attention module (CBAM), which could accurately extract the characteristics of the partial wear state of the brake pad with an accuracy rate of 99.89%. There are many studies on the wear and wear state of Cu-based PM brake pads but few studies focused on the wear rate prediction of Cu-based PM brake pad.

Aiming at the above problems, this paper takes the Cu-based PM brake pad (hereinafter referred to as the brake pad) as the research object, and its friction performance tests with different braking conditions were based on the 1:1 brake bench. According to the test results, we discussed the variation trend and the change mechanism of friction coefficient, temperature, braking distance, wear rate of brake pad with multi-factor coupling conditions. Furthermore, the wear rate of the brake pad is predicted based on the Atom Search Optimization-Back Propagation (ASO-BP) method.

2. Test design

In order to accurately obtain the performance data of the brake pad with different braking conditions, we carried out the braking test by the ZJZ (JP) 117 model 1:1 braking power test bench. The schematic diagram of test platform is shown in Fig. 1.

During testing, the test equipment is controlled by the control system F, and motor A provides the rotating power for the brake disc G, so that the initial braking speed reaches the predetermined value of the test, then the brake caliper H is driven by the hydraulic pump C to give pressure to the brake pad I, make the brake pad rub with the brake disc,

Table 1
Raw material and mass fraction of brake pad preparation.

Item	Matrix component			Friction component		Lubricant component	
Component	Cu	Fe	Cr	SiO_2	Al_2O_3	MoS_2	graphite
Content (wt%)	55	10	8	7	5	5	10

flywheel group B is used to replace train inertia to simulate train braking.

It is necessary to design the test braking conditions for accurately simulating the actual braking conditions:

1) In order to simulate the braking of the train under normal weather conditions, the braking test with normal temperature and dry conditions is designed;
2) In order to simulate the braking of the train in rainy weather, the braking test with normal temperature and humidity is designed;

Fig. 2. Prepared copper-based powder metallurgy brake pad.

Table 2
Physical parameters of copper-based brake pad and brake disc.

Physical parameters	Brake pad	Brake disc
Friction pad density	5 g/cm^3	7.85 g/cm^3
HardnessHBW10/250/30	18.5HBW	>290HBW
Shear strength	11.8 MPa	–
Tensile strength	610 MPa (back plate)	1130 MPa
Young's modulus	–	210 GPa
Al + Si content	0.3%	–
Cr + Zr + W content	<2%	–
Thermal conductivity	52 W/(m·K)	45 W/(m·K)
Specific heat capacity	900 J/(kg·K)	563 J/(kg·K)
Poisson's ratio	0.3	0.32

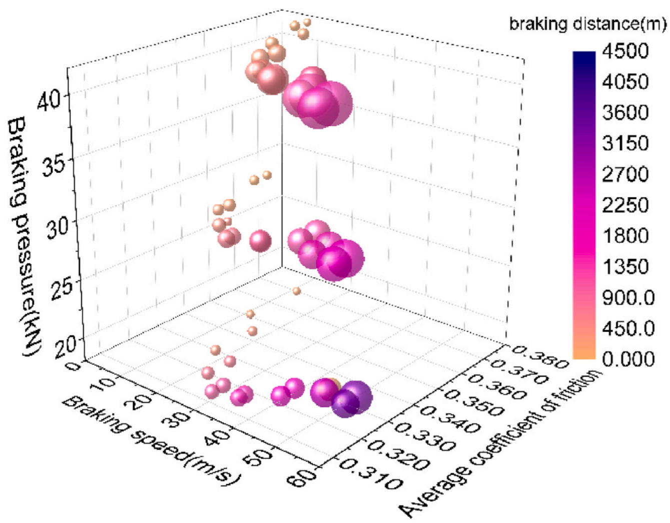

Fig. 3. Coupling diagram of multiple braking conditions under dry.

3) In order to simulate the situation of train speed control and braking on the downhill, the continuous braking test on the ramp is designed;
4) In order to simulate the empty and heavy-load conditions of the train during braking, the braking test of the heavy-load train (18t) and the empty train (13t) is designed with normal temperature and dry state;
5) The brake pad has a pre-grinding stage and a stable wear stage in the friction process. In order to achieve a comparative effect, the braking test in a dry state and normal temperature after pre-grinding is designed.
6) SEM and energy spectrum analysis of the brake pad are carried out.

During testing, the damp condition is provided by the water tank D for the braking device, since the real-time data of the surface temperature of the brake pad cannot be obtained, the infrared thermometer E is used to measure the surface temperature of the brake disc instead of the brake pad.

The raw materials and mass fraction of Cu-based PM brake pads for the test are shown in Table 1. The brake pad for the test is shown in Fig. 2. The physical parameters of the brake pad and brake disc for the test are shown in Table 2.

In order to measure the wear rate, we weighing the brake pad before and after each test procedure, and the wear rate can be calculated by formula (1):

$$Q = \frac{M_a - M_b}{\rho \cdot W} \tag{1}$$

Where, Q is the wear rate of the brake pad, the unit is cm^3/MJ; M_a and M_b are the weight before the test and after the test respectively, the unit is g; ρ is the density of friction block of brake pad, the unit is g/cm^3; W is the total braking work of braking test, the unit is MJ.

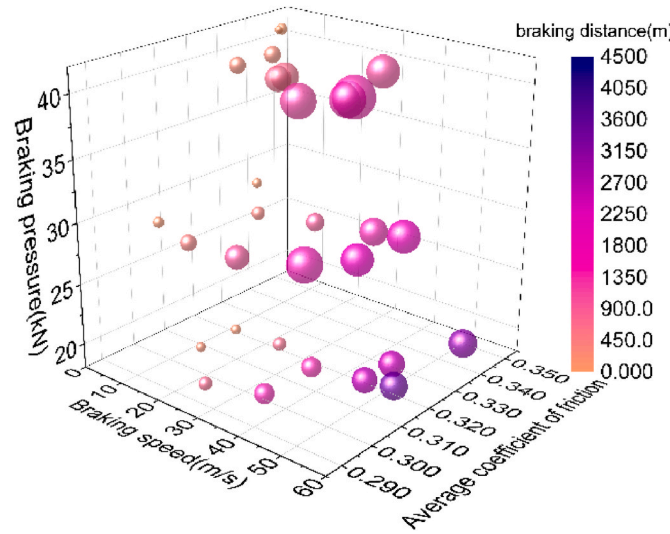

Fig. 4. Coupling diagram of multiple braking conditions under wet.

Table 3
Braking tests conditions.

Braking tests conditions	Range
Braking speed	0–50 m/s
Braking pressure	18 kN, 30 kN, and 42 kN
Environmental factor	Wet and dry

3. Analysis of friction performance of brake pad with different braking conditions

During the actual braking process of the train, the braking capacity of the brake pad is affected by various factors, Fig. 3 and Fig. 4 are the coupling schematic diagrams of braking speed, braking pressure, braking distance, temperature, and average friction coefficient with dry and wet conditions respectively.

The specific braking test conditions are shown in Table 3. In Figs. 3 and 4, the size of the sphere in the figure represents the temperature of the brake pad at the end of braking, and the shade of the color represents the braking distance. And when the braking speed is constant and the braking pressure is smaller, the brake pad's friction temperature performs lower, and the braking distance becomes longer. When the braking pressure is constant and the braking speed is greater, the brake pad's friction temperature performs higher, and the braking distance becomes shorter.

3.1. Influence of different braking conditions on the average friction coefficient of brake pad

Fig. 5 shows the variation of the friction coefficient of the brake pad with different braking conditions. It can be seen from Fig. 5(a) and (e) that the average friction coefficient of the brake pad decreases with the increase of the braking speed, and the instantaneous friction coefficient fluctuates between 0.3 and 0.5, when the braking pressure is 18 kN and the braking speed is less than 33.3 m/s with dry conditions. The average friction coefficient increases with the increase of braking speed, and the instantaneous friction coefficient fluctuates between 0.31 and 0.43, when the braking speed is more than 33.3 m/s. This is because the micro-protrusions on the surface of the brake pad have a strong shear resistance and a hard texture, as shown in Fig. 6 (a), and the friction coefficient shows a high value, when the braking speed is lower. When the speed increases, the micro-protrusions on the surface of the brake pad is destroyed, as shown in Fig. 6 (b), which results in the friction

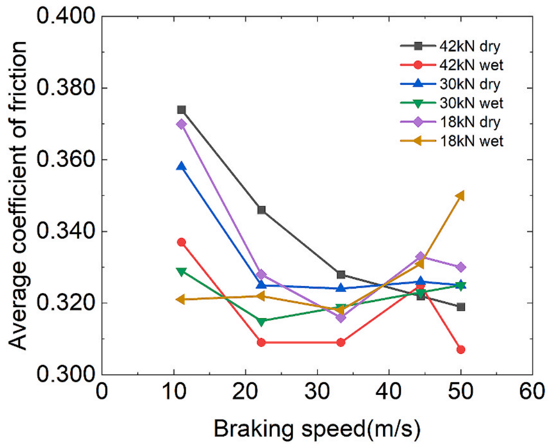

(a) Average friction coefficient as a function of braking speed

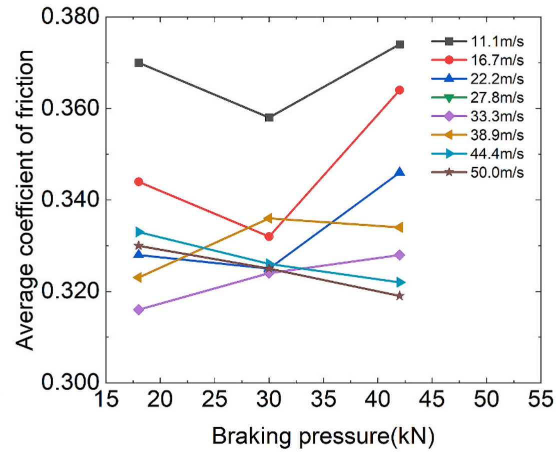

(b) Average friction coefficient as a function of brake pressure

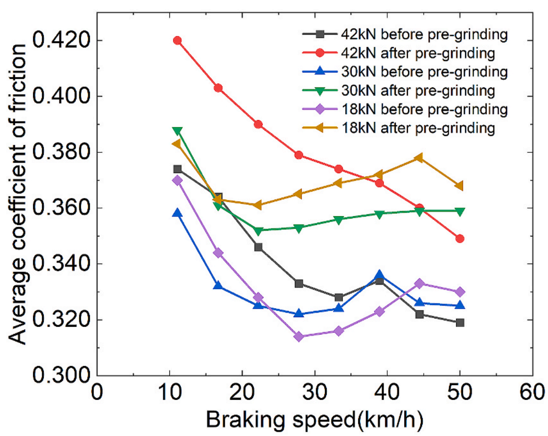

(c) Comparison of average friction coefficients before and after brake pad pre-grinding

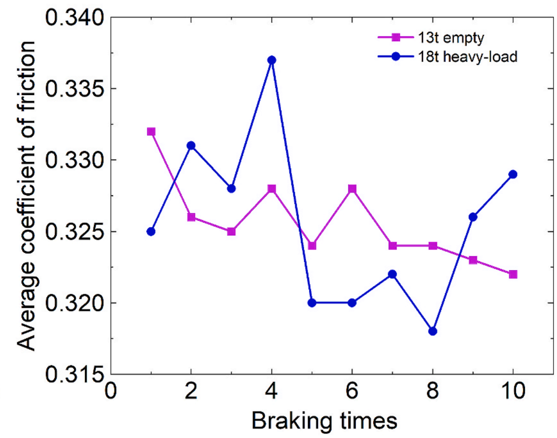

(d) Comparison of the average friction coefficient of empty and heavy trains

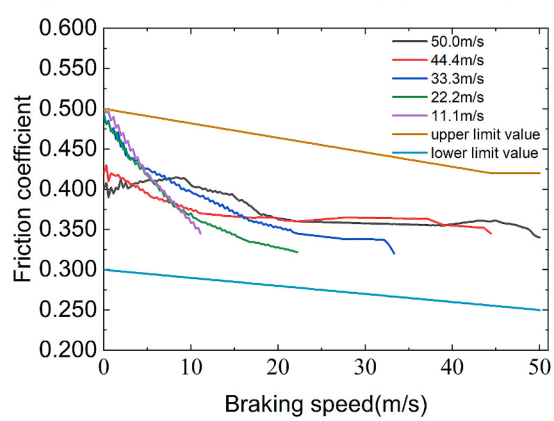

(e) Variation of instantaneous friction coefficient with speed

Fig. 5. Variation of average friction coefficient of brake pad under different braking conditions.

coefficient decreasing. At high speed, the micro-protrusions on the surface of the brake pad are smoothed, as shown in Fig. 6 (c), so that the frictional contact area between the brake pad and the brake disc increases, and the friction coefficient increases. Under the dry working condition, with the increases of braking pressure and braking speed, the average friction coefficient of the brake pad decreases first and then tends to be stable. Through the energy spectrum analysis of the brake pad surface before and after braking, as shown in Fig. 7, it can be seen that the oxygen content in the energy spectrum increases, which indicates that the third body "oxide film" [23] is formed on the friction surface, and the "oxide film" can stabilize the friction coefficient and play a lubricating role.

As shown in Fig. 5(a), with wet conditions and the braking pressure of 18 kN, when the speed is less than 33.3 m/s, the average friction coefficient is relatively stable, because the water film is formed on the surface of the brake pad which can play a lubricating role. When the

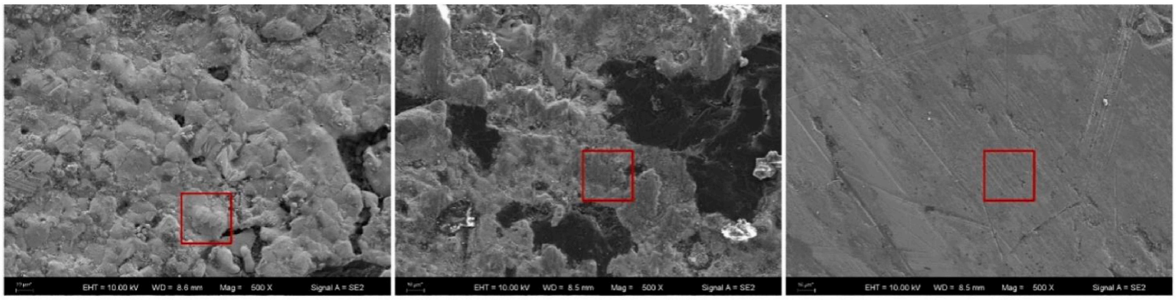

(a) Micro-protrusions before braking (b) Micro-protrusions destroyed (c) Micro-protrusions are smoothed

Fig. 6. Surface microscopic changes before and after brake pad wear.

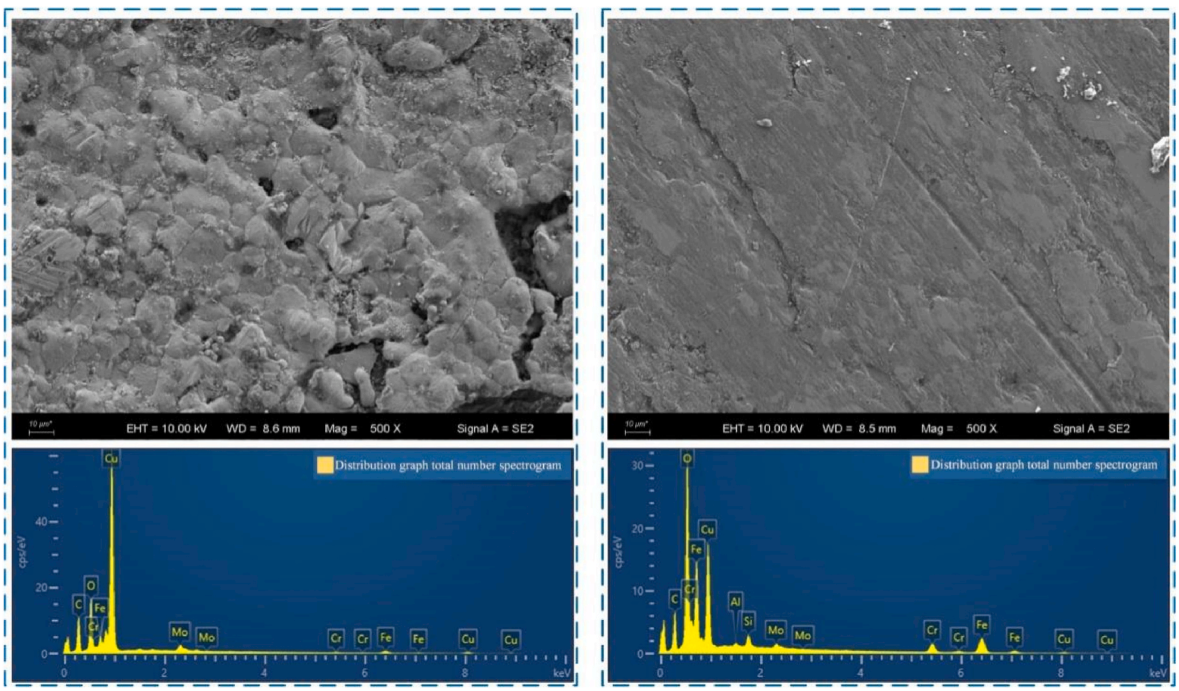

Fig. 7. Energy spectrum diagram of brake pad surface before and after braking.

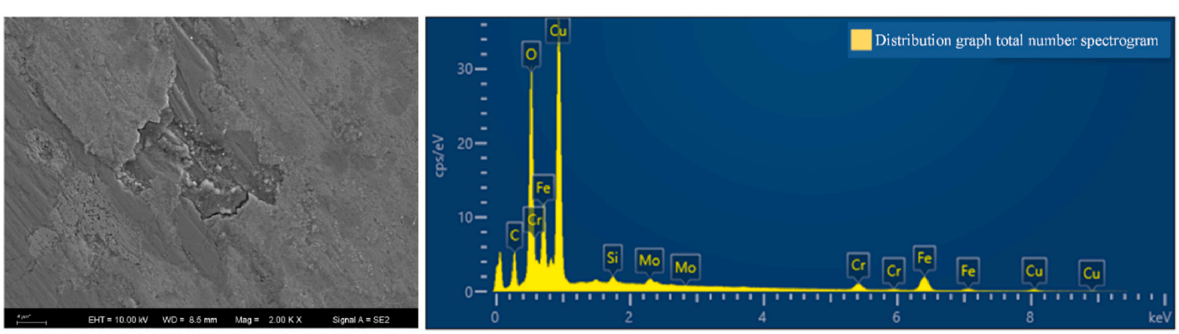

Fig. 8. Surface and energy spectrum analysis of brake pad after braking.

speed is more than 33.3 m/s, the water film on the friction surface is destroyed, thus losing the lubrication, and the average friction coefficient increases with the increase of speed. With wet conditions and 30 kN braking pressure, when the speed is less than 22.2 m/s, the water film is not stable, and the average friction coefficient decreases with the increasing speed. When the speed is more than 22.2 m/s, the average friction coefficient increases gradually with the increasing speed, the reason is that the water film cannot be formed due to the water evaporation at high-temperature. With wet conditions, when the braking pressure is 42 kN, the average friction coefficient first decreases and then tends to be stable, because the braking speed increases, the water film gradually loses its effect, meanwhile the 'oxide film' of the brake pad surface is formed according to the energy spectrum of the brake pad surface after friction, as shown in Fig. 8.

Table 4
Average friction coefficient and temperature of brake pad under continuous braking conditions.

Conditions	Brake conditions			Result	
	Power (kW)	Speed (m/s)	Time (min)	Average coefficient of friction	Maximum temperature
Continuous braking	20	22.2	20	0.394	207 °C
	65	44.4	15	0.345	473 °C
	30	22.2	20	0.399	289 °C

It can also be seen from Fig. 5(a) that the average friction coefficient is generally small at low speed due to the existing moisture with wet conditions. However, at high speed, the moisture evaporates rapidly due to high-temperature, so the difference between the average friction coefficients with dry and wet conditions becomes smaller. Fig. 5(b) shows that the average friction coefficient first decreases and then increases at low speed, when the brake pressure increases. When the speed reaches 27.8 m/s, the increasing brake pressure leads to the increases of average friction coefficient. As the increases of braking speed, the average friction coefficient of the brake pad gradually decreases with the braking pressure. Fig. 5(c) is a comparison diagram of the difference of the average friction coefficient before and after the brake pad pre-grinding. It can be seen that the average friction coefficient of the brake pad after pre-grinding is higher than before, and the average friction coefficient after pre-grinding is relatively stable with the braking speed increase. Because the surface of the brake pad before pre-grinding has more micro-protrusions, as shown in Fig. 6(a), the brake pad can not contact fully with the brake disc, and the friction coefficient shows a small value. After pre-grinding, the surface of the brake pad is destroyed, as shown in Fig. 6(b), the contact area between the surface of the brake pad and the brake disc increases, and the friction coefficient shows a higher value. Fig. 5(d) shows two braking conditions of the empty train (13t) and the heavy-load train (18t), when the braking speed is 44.4 m/s and the braking pressure is 42 kN, compared the empty train with the heavy-load train the average friction coefficient of the brake pad fluctuates more obviously.

During the operation of the train, it usually encounters downhill, the train needs to continuously brake to maintain the speed within a safe range. Table 4 gives the average friction coefficient and temperature of the brake pad with different conditions of continuous braking. According to Table 4, when the speed is 22.2 m/s and the braking power is low, the average friction coefficient is more than 0.39, but when the speed and braking power increase, the average friction coefficient decreases to 0.345. The reasons for this change are as follows: (1) At low power and low speed, the heat produced by friction is limited, and the matrix strength of the brake pad is basically unchanged, as shown in Fig. 9(a), so the average friction coefficient shows a higher value. (2) At high power and high speed, a large amount of heat is generated by friction, which softens the matrix of the copper-based brake pad, as shown in Fig. 9(b), the darker color of area A in the figure indicates that the "oxide film" is formed on the surface of the brake pad, so that the average friction coefficient shows a lower value.

3.2. *Influences of different braking conditions on friction temperature and braking distance*

During the braking process of the train, the brake pad and the brake disc will generate heat due to friction, which will affect the braking performance of the brake pad. Therefore, in the actual braking process, it is necessary to cool the brake disc and brake pad. Fig. 10(a) shows the variation of brake pad friction temperature with the braking speed in dry and wet braking conditions. At the same braking pressure and the small braking speed, the temperature generated by braking with wet conditions is lower than dry, because the presence of moisture can play a role in cooling down. However, when the speed reaches 50 m/s, the water evaporates quickly due to the high temperature generated by braking, so the water cannot exist on the friction surface, and the cooling effect is weakened. Therefore, at high speed, the temperature of the brake pad with the two braking conditions is basically same.

Fig. 10(b) and (c) respectively show the variation of braking distance and braking time with braking speed in different working conditions. Combining Fig. 10(b) with Fig. 10(c), the braking distance and braking time with wet conditions are longer than dry, which indicates that moisture plays a role in lubrication. Combining Fig. 10(a), (b) and (c), it can be seen that the brake pad temperature with dry, 42 kN, 50 m/s braking conditions is 28 °C higher than dry, 30 kN, 50 m/s, and 46 °C higher than with dry, 18 kN, 50 m/s. The braking distance with dry, 42 kN, 50 m/s braking conditions is 582 m less than with dry, 30 kN, 50 m/s, and 1945 m less than with dry, 18 kN, 50 m/s. The braking time with dry, 42 kN, 50 m/s braking conditions is 23.3 s less than with dry, 30 kN, 50 m/s, and 79.4 s less than with dry, 18 kN, 50 m/s. Fig. 10(d) shows the results of the braking test with dry, 42 kN, and 44.4 m/s conditions, it can be seen that compare the heavy-load train with the empty, the friction temperature of the brake pad is higher and the braking distance is longer.

Different braking conditions have a significant impact on the temperature, distance, and time generated by braking. Therefore, in the

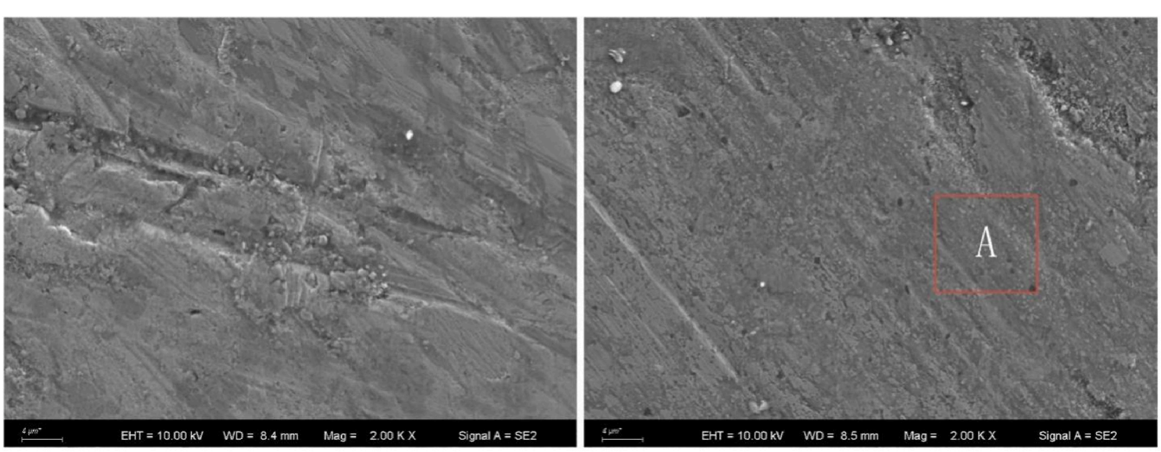

(a) Surface appearance of brake pad after low power and low speed braking (b) Surface Appearance of Brake Pad high power and high speed braking

Fig. 9. SEM diagram of brake pad surface after continuous braking.

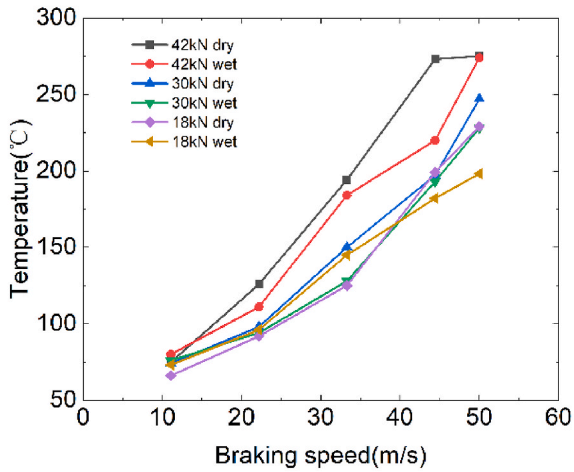

(a) Friction temperature as a function of speed

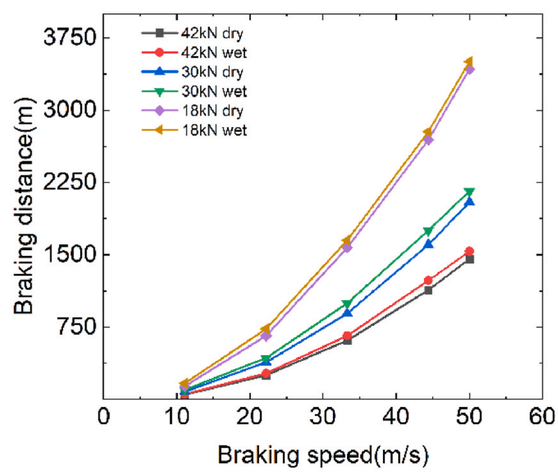

(b) Braking distance varies with speed

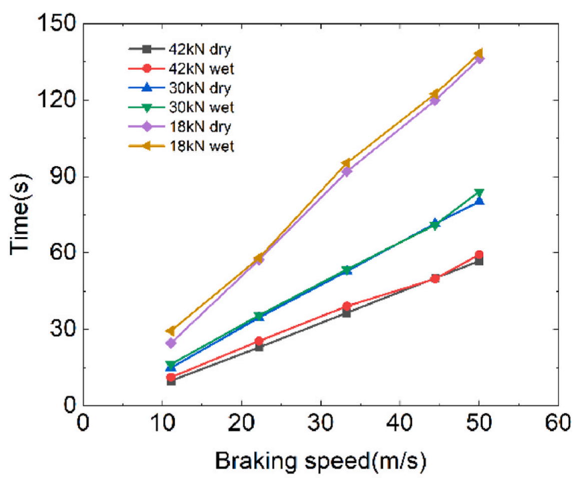

(c) Braking time varies with speed

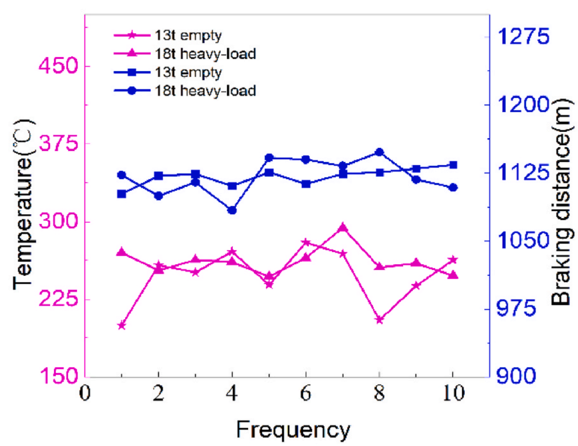

(d) Changes in friction temperature and braking distance under empty and heavy train conditions

Fig. 10. Changes of friction temperature and braking distance under different working conditions.

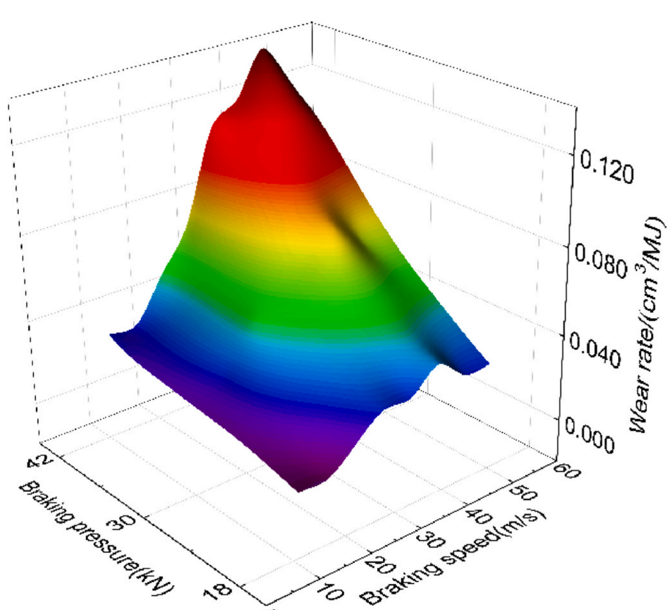

Fig. 11. Changes of wear rate under different braking conditions.

actual braking process, the train driver should make a corresponding judgment according to the actual situation and execute the braking to reduce the risk rate caused by braking.

3.3. Influences of different braking conditions on the wear rate of brake pad

In the process of train braking, the braking speed and pressure are important to the wear rate. Fig. 11 shows the change of wear rate with different braking conditions. It can be seen that under a certain braking pressure, the wear rate continues to increase with the increase of speed at low speed, because the surface of the brake pad is relatively rough; At high speed, the wear rate of the brake pad is reduced and tends to be stable, this is because the friction between the brake pad and the brake disc generates more heat to form an oxide film on the surface of the brake pad. When the braking speed is constant, as the braking pressure increases, the wear rate of the brake pad shows a trend of continuous increase.

To further study the change of the wear rate, we predict the brake pad wear rate by the ASO-BP neural network algorithm, and compare the predicted results with the BP neural network algorithm.

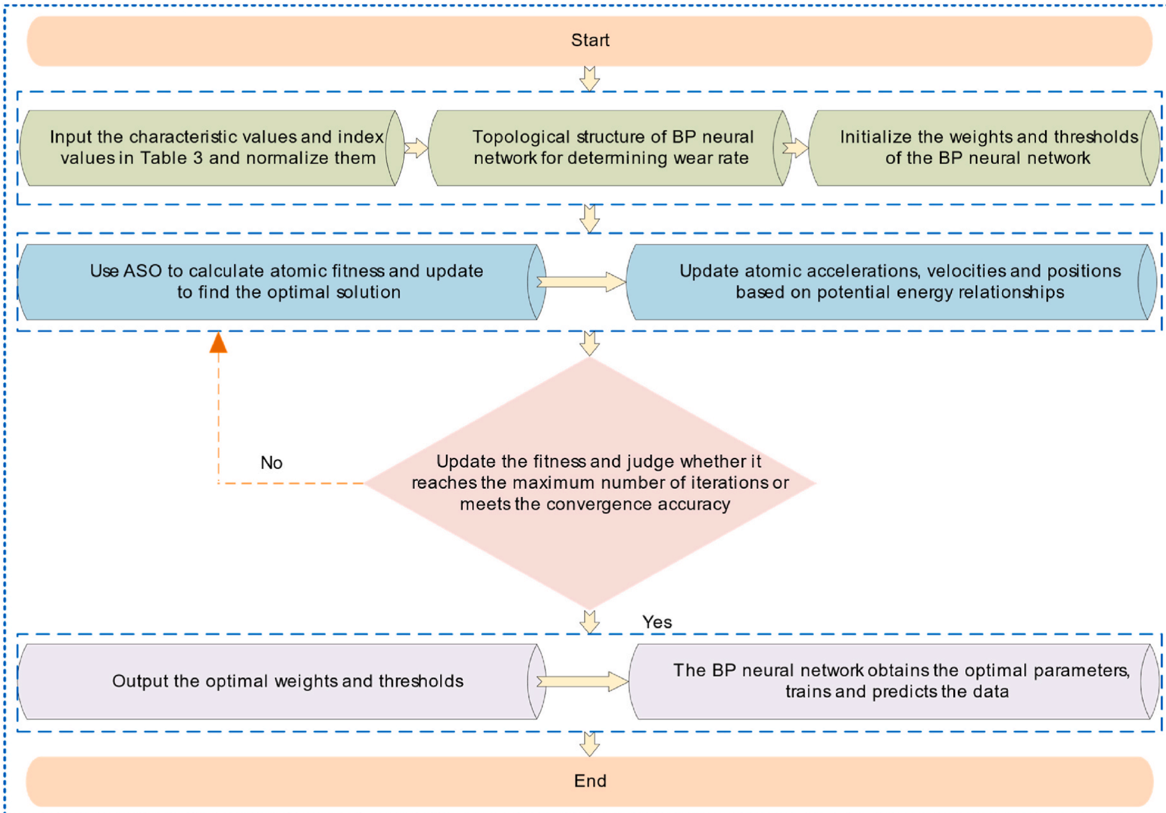

Fig. 12. Flow chart of brake pad wear rate prediction based on ASO-BP.

4. Wear rate prediction based on ASO-BP neural network

4.1. Principle of ASO

The ASO guides the optimization search through the interaction force and system constraint between atoms, and has the advantages of fast convergence speed and strong optimization ability [24]. ASO is a model based on molecular dynamics, and the motion of atoms follows Newton's second law, formula (2):

$$a_i(t) = \frac{F_i(t) + G_i(t)}{m_i t} \tag{2}$$

Where: $a_i(t)$ is the acceleration of the i atom at the t iteration; $F_i(t)$ is the interaction force of the i atom at the t iteration; $G_i(t)$ is the binding force of the i atom at the t iteration; $m_i(t)$ represents the mass of the i atom. $F_i(t)$ can be regarded as the random weighted sum of the force of k atoms with better fitness function values on the i atom, such as formulas (3)-(8):

$$F_i(t) = \sum_{j \in K_{best}} rand_j F_{ij}(t) \tag{3}$$

$$K_{best} = S - (S-2)\cdot\sqrt{\frac{t}{t_{\max}}} \tag{4}$$

$$F_{ij}(t) = -n(t)\left[2\left(h_{ij}(t)\right)^{13} - \left(h_{ij}(t)\right)^{7}\right] \tag{5}$$

$$-n(t) = -\alpha\left(1 - \frac{t-1}{t_{\max}}\right)^{3} e^{-20t/t_{\max}} \tag{6}$$

$$h_{ij}(t) = \begin{cases} h_{\min}, r_{ij}(t)/\sigma(t) < h_{\min} \\ r_{ij}(t)/\sigma(t), h_{\min} < r_{ij}(t)/\sigma(t) \le h_{\max} \\ h_{\max}, r_{ij}(t)/\sigma(t) > h_{\max} \end{cases} \tag{7}$$

$$\begin{cases} r_{ij} = \left\|X_i(t), X_j(t)\right\|_2 \\ \sigma(t) = \left\|X_i(t), \sum_{j \in K_{best}} \frac{X_j(t)}{K(t)}\right\|_2 \end{cases} \tag{8}$$

Where: The value range of $rand_j$ is [0,1]; $F_{ij}(t)$ is the potential energy of the j atom to the i atom at the t iteration; K_{best} is the set of forces acting on atom i; S is the total number of atoms; t_{max} is the total number of iterations; $n(t)$ is the range that can adjust the attractive and repulsive regions; α is the depth weighting; h_{ij} is the distance between i and j atoms; $h_{\min} = \varepsilon_0 + \varepsilon(t)$ is the lower bound of h; $\varepsilon(t)$ is the drift factor with the number of iterations; h_{max} is the upper bound; X_i and X_j are atoms are the positions of i and j respectively; $\sigma(t)$ is the range of distances between atoms in the K_{best} set from the i atom.

In molecular mechanics models, atomic motions are geometrically constrained, in ASO, it is assumed that each atom has a covalent bond with the optimal atom, so the binding force of the optimal atom acts on each atom, so $G_i(t)$ in formula (2) expressed as formulas (9)-(10):

$$G_i(t) = \lambda(t)(X_{best}(t) - X_i(t)) \tag{9}$$

$$\lambda(t) = \beta e^{-20t/t\ \max} \tag{10}$$

Where: $\lambda(t)$ is an adaptive adjustment parameter; β is the multiplier weight.

$m_i(t)$ in formula (2) is expressed as formula (11):

$$\begin{aligned} m_i(t) &= \frac{M_i(t)}{\sum_{j=1}^{N} M_j(t)} \\ M_i(t) &= e^{-\frac{g_i(t) - g_{\min}(t)}{g_{\max}(t) - g_{\min}(t)}} \end{aligned} \tag{11}$$

Where: $g_i(t)$ is the fitness value of the i atom; $g_{\max}(t)$ and $g_{\min}(t)$ are the

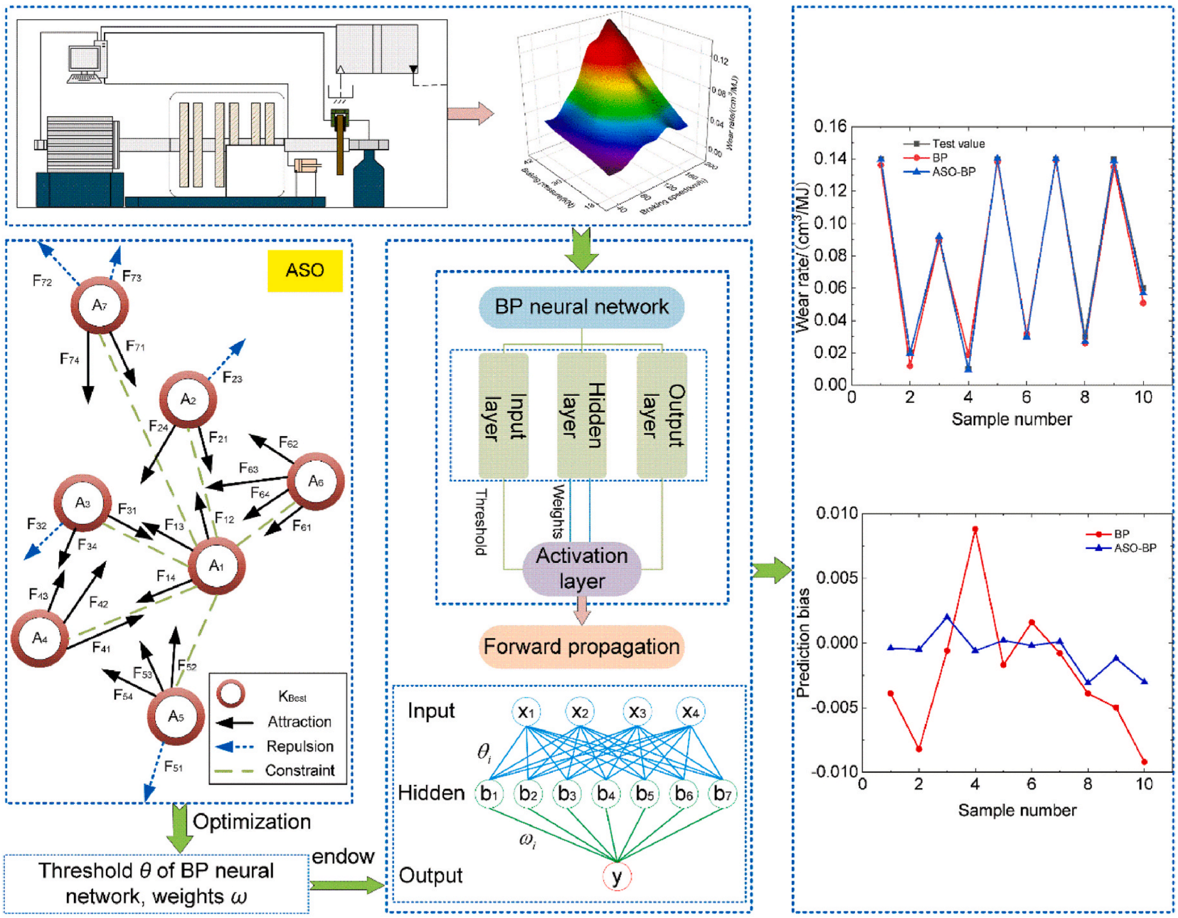

Fig. 13. Prediction framework of powder metallurgy brake pad wear rate.

maximum and minimum fitness values in the atomic population respectively.

Then the acceleration of the i atom during t iterations is formula (12):

$$a_i(t) = \frac{F_i(t) + G_i(t)}{m_i^d(t)}$$
$$= -\alpha\left(1 - \frac{t-1}{t_{\max}}\right)^3 e^{\frac{-20t}{t_{\max}}} \sum_{j \in K_{best}} \frac{rand_j\left[2\left(h_{ij}(t)\right)^{13} - \left(h_{ij}(t)\right)^7\right]}{m_i(t)}$$
$$+\beta e^{\frac{-20t}{t_{\max}}} \frac{\left(X_{best}(t) - X_i(t)\right)}{m_i(t)} \quad (12)$$

The acceleration changes the position of the atom, and through each iteration update, the velocity and position of the atom i is obtained, as shown in formula (13):

$$\begin{aligned} v_i(t+1) &= rand_i v_u(t) + a_i(t) \\ x_i(t+1) &= x_i(t) + v_i(t+1) \end{aligned} \quad (13)$$

4.2. Wear rate prediction method based on ASO-BP neural network

The BP neural network has some disadvantages, such as slow convergence speed, easy convergence of weight to local minima, lower prediction accuracy, easily leading to network training failure, etc. [25], therefore, the ASO algorithm is used in this paper to optimize the BP neural network, and the ASO-BP neural network is used to predict the wear rate of the brake pad.

Firstly, we use the BP neural network algorithm to preprocess the eigenvalues and index values in Table 3 to obtain the initial threshold and weight values; Secondly, we use ASO to optimize the initial threshold and weight values, and return to the BP neural network after optimization; Finally, we predict the wear rate.

Fig. 12 shows the predicting process of the wear rate of the brake pad based on the ASO-BP neural network.

Table 5
Sample data.

Sample number	Feature1	Feature2	Feature3	Feature4	Target
1	44.4	42	1134	0.322	0.140
2	44.4	42	1115	0.328	0.140
3	33.3	18	1561	0.318	0.030
4	50.0	18	3388	0.334	0.040
5	16.7	30	202	0.336	0.020
…	…	…	…	…	…
75	27.8	30	617	0.322	0.060

4.3. ASO-BP prediction results

The wear rate prediction framework based on ASO-BP neural network is shown in Fig. 13.

In the process of ASO optimizing the BP neural network, the maximum evolutionary algebra is set to 100, the initial population size is set to 30, and the population fitness function is shown in formula (14):

$$F = \min\left(MSE_{TrainingSet, TestingSet}\right) \quad (14)$$

Where: *TrainingSet* and *TestingSet* are the characteristic values of brake pad wear rate of the training set and the test set respectively, and *MSE* is the mean square error.

Through the test of 5 different working conditions, the sample data containing 4 eigenvalues and 1 index value are obtained, as shown in

Table 6
Test data.

Sample number	Feature1	Feature2	Feature3	Feature4	Target
1	44.4	42	1136	0.323	0.140
2	22.2	18	660	0.328	0.020
3	33.3	36	739	0.322	0.090
4	16.7	18	364	0.330	0.010
5	44.4	42	1113	0.328	0.140
6	16.7	42	125	0.364	0.030
7	44.4	42	1100	0.331	0.140
8	11.1	42	49	0.374	0.030
9	44.4	42	1140	0.320	0.140
10	27.8	30	617	0.322	0.060

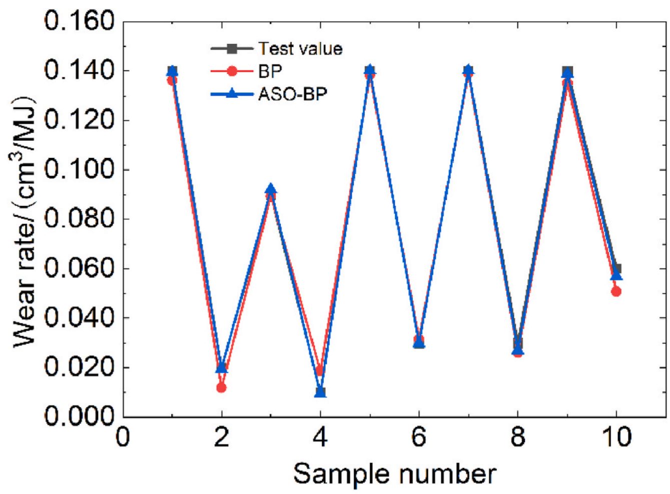

Fig. 14. Comparison between the predicted value of BP neural network before and after ASO optimization and the actual value.

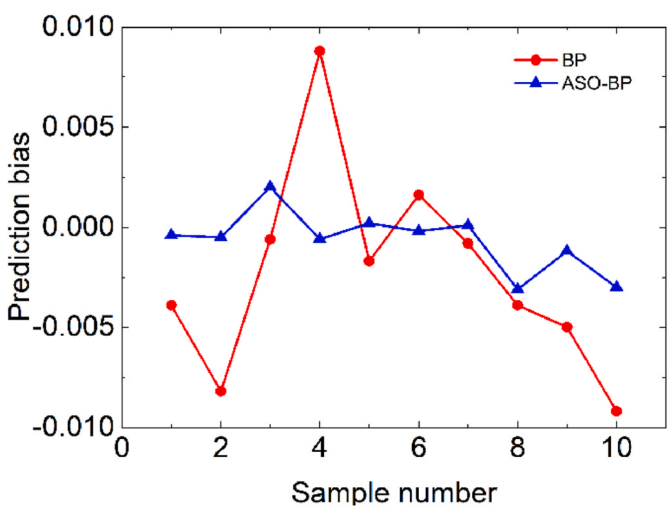

Fig. 15. Comparison of error between the predicted value and real value of BP neural network before and after ASO optimization.

Table 5. The feature values are braking speed (Feature1), braking pressure (Feature2), braking distance (Feature3), and average friction coefficient (Feature4), and the index value is the wear rate (Target). The actual data is divided into 75 groups, since the brake pad wear rate data is a small sample [26], in order to make the prediction results as accurate as possible, multiple sets of training data and test data are selected and the prediction results are compared, as shown in Table 7, it can be seen that when 65 groups are used as training data and 10 groups are used as testing data, the results are optimal. Therefore, using ASO-BP and BP two algorithms to train 65 sets of data, in order to achieve the comparison effect, the hidden layers of the neural network of the two algorithms are both 7 layers, and the test data in Table 6 is used for verification, the prediction results are shown in Fig. 14 and Fig. 15.

It can be seen from Figs. 14 and 15 that compare the prediction results using the BP neural network with the actual, the absolute value of the minimum deviation of the prediction is 0.000800 and the maximum 0.00920. However, compare the prediction result of the ASO-BP neural network with the actual, the absolute value of the minimum deviation of the prediction is only 0.000100 and the maximum is 0.00310.

The comparisons of the indicators predicted by the two algorithms, ASO-BP and BP, are shown in Table 7. From Table 7 it can be seen that the 65 groups training data and 10 groups testing data is the optimal results. The accuracy of ASO-BP is 14.5% higher than that of BP, the mean square error is only 8.49% of BP, and the average absolute percentage error is 14.4% less than that of BP. In conclusion, ASO-BP neural network is better than the traditional BP neural network in predicting the wear rate of the brake pad.

The above prediction is carried out with dry conditions. However, as long as sufficient data can be obtained for training with other conditions, ASO-BP can also predict the wear rate of brake pads with multiple conditions. The prediction of wear rate of brake pad by ASO-BP can provide a reference for the replacement of brake pad in service and the improvement of its life.

5. Conclusion

This paper explores the friction coefficient, friction temperature, braking distance, braking time, wear mechanism and wear rate of Cu-based PM brake pads with multi-factor coupling conditions. Meanwhile, the wear rate of the brake pad is predicted. The conclusions of this study are drawn as follows:

(1) Braking speed, braking pressure, environmental humidity, and empty and heavy-load conditions affect the friction coefficient, friction temperature, and braking distance of Cu-based PM brake pads.
(2) With the change of braking speed and braking pressure, the average friction coefficient of the brake pad fluctuates between 0.3 and 0.45, the maximum of temperature, braking distance, braking time and the wear rate of the brake pad are 473 °C, 3506 m, 138s and 0.14 cm^3/MJ, respectively.
(3) The prediction result of wear rate of brake pads can reach 97.3% based on ASO-BP neural network, which is 14.5% higher than the BP neural network. ASO-BP neural network algorithm is suitable for small sample, and its application is not limited to wear rate prediction, such as failure prediction and other fields.

Future work will focus on discussing the friction performance and the change mechanism of the brake pad with the conditions of vibration, high cold weather, sediment, and the empty and load trains.

The method proposed in this paper is also applicable to development and the trial production stage of brake pads.

Funding

This work was supported by the National Natural Science Foundation of China (Grant numbers [79970045] and [61179023]).

Author statement

Jiawei Chen: Methodology, Validation, Experimental work, Writing - Original Draft.

Chunyu Yu: Experimental work, Writing - Review and Editing, Funding Acquisition, Supervision.

Table 7
Comparison of ASO-BP prediction and BP prediction.

Evaluation indicators	65 groups training data, 10 groups testing data		60 groups training data, 15 groups testing data		70 groups training data, 5 groups testing data	
	BP prediction	ASO-BP prediction	BP prediction	ASO-BP prediction	BP prediction	ASO-BP prediction
Accuracy	82.8%	97.3%	87.2%	95.4%	86.8%	95.1%
Mean absolute error (MAE)	0.00438	0.00113	0.00341	0.00132	0.00468	0.00195
Mean square error (MSE)	0.0000292	0.00000248	0.0000176	0.00000433	0.0000346	0.00000585
Mean absolute percentage error (MAPE)	17.2%	2.79%	13.0%	4.72%	13.2%	4.82%

Qi Cheng: Review and Editing.
Yuanlin Guan:Review and Editing.
Qinghai Zhang: Review and Editing.
Weipu Li: Experimental work.
Fuhao Ouyang: Experimental work.
Zhenning Wang: Provision of experimental materials.

Declaration of competing interest

The authors declare that they have no known competing financial interests or personal relationships that could have appeared to influence the work reported in this paper.

Data availability

Data will be made available on request.

References

[1] L. Wang, Q.R. Pan, S. Zhu, S.Z. Wu, Fabrication of copper-based powder metallurgy brake pad for high speed train and its friction and wear property, Mater. Mech. Eng. 41 (6) (2017) 55–58, https://doi.org/10.11973/jxgccl201706013.

[2] L.H. Qi, J. Liu, J.T. Guan, H. Li, Tensile properties and damage behaviors of Csf/Mg composite at elevated temperature and containing a small fraction of liquid, Compos. Sci. Technol. 72 (9) (2012) 1774–1780, https://doi.org/10.1016/j.compscitech.2012.07.014.

[3] X.Y. Wang, H.Q. Ru, Braking properties of Cu-Fe based powder metallurgy braking materials, Powder Metall. Ind. 25 (6) (2015) 48–52, https://doi.org/10.13228/j.boyuan.issn1006-6543.20150022.

[4] P.F. Gao, H. Yang, X.G. Fan, P.H. Li, Quick prediction of the folding defect in transitional region during isothermal local loading forming of titanium alloy large-scale rib-web component based on folding index, J. Mater. Process. Technol. 219 (2015) 101–111, https://doi.org/10.1016/j.jmatprotec.2014.11.047.

[5] A. Akbarzadeh, S. Naghdy, Hot workability of a high carbon high chromium tool steel, Mater. Des. 46 (11) (2013) 654–659, https://doi.org/10.1016/j.matdes.2012.10.055.

[6] P. Zhang, L. Zhang, K.X. Fu, P.F. Wu, J.W. Cao, C.R. Shijia, X.H. Qu, The effect of Al_2O_3 fiber additive on braking performance of copper-based brake pads utilized in high-speed railway train, Tribol. Int. 135 (2019) 444–456, https://doi.org/10.1016/j.triboint.2019.03.034.

[7] V. Chauhan, J. Bijwe, A. Darpe, Functionalization of alumina particles to improve the performance of eco-friendly brake-pads, Friction 9 (5) (2021) 1213–1226, https://doi.org/10.1007/s40544-020-0461-5.

[8] T. Peng, Q.Z. Yan, X.L. Zhang, Y. Zhuang, Role of titanium carbide and alumina on the friction increment for cu-based metallic brake pads under different initial braking speeds, Friction 9 (6) (2021) 1543–1557, https://doi.org/10.1007/s40544-020-0439-3.

[9] S. Kumar, S.K. Ghosh, Porosity and tribological performance analysis on new developed metal matrix composite for brake pad materials, J. Manuf. Process. 59 (2020) 186–204, https://doi.org/10.1016/j.jmapro.2020.09.053.

[10] G.K. Gyimah, P. Huang, D. Chen, Dry sliding wear studies of copper-based powder metallurgy brake materials, J. Tribol. 136 (4) (2014), 041601, https://doi.org/10.1115/1.4027477.

[11] J.X. Liu, L.L. Sun, J.L. Fan, S. Wu, Y. Wang, Y. Li, Effect of forming properties of cu-based powder metallurgy friction materials, Nonferrous Met. 1 (2019) 64–67. CNKI:SUN:METE.0.2019-01-014.

[12] Z.Y. Xiang, Z.Y. Fan, Q. Liu, Y.K. Wu, J.L. Mo, Z.R. Zhou, Effect of brake pad friction block shape on tribological behavior of brake interface of high-speed train, Tribology 41 (2021) 95–104, https://doi.org/10.16078/j.tribology.2020038, 01.

[13] J.Y. Yang, F. Gao, Y. Sun, X.M. Han, Influence of geometry of brake pad on disc temperature and friction performance, Chin. J. Nonferrous Metals 28 (2018) 1351–1360, https://doi.org/10.19476/j.ysxb.1004.0609.2018.07.10, 07.

[14] H.J. Noh, H. Jang, Friction instability induced by iron and iron oxides on friction material surface, Wear 400 (2018) 93–99, https://doi.org/10.1016/j.wear.2017.12.025.

[15] Y. He, G.X. Chen, J. Zhang, X.F. Zhang, Q.F. Qiao, X.B. Xiao, Influence of braking pressure on abnormal braking noise of an intercity train, 01, Noise Vib. Contr. 40 (2020) 116–121+137. CNKI:SUN:ZSZK.0.2020-01-022.

[16] K.I. Kim, H. Lee, J. Kim, K.H. Oh, K.T. Kim, Wear behavior of commercial copper-based aircraft brake pads fabricated under different SPS conditions[J], Crystals 11 (11) (2021) 1298, https://doi.org/10.3390/cryst11111298.

[17] G.S. Krishnan, L.G. Babu, P. Kumaran, G. Yoganjaneyulu, J.S. Raj, Investigation of Caryota urens fibers on physical, chemical, mechanical and tribological properties for brake pad applications, Mater. Res. Express 7 (2020), 015310, https://doi.org/10.1088/2053-1591/ab5d5b, 01.

[18] X. Ma, C.H. Luan, S.W. Fan, J.L. Deng, L.T. Zhang, L.F. Cheng, Comparison of braking behaviors between iron- and copper-based powder metallurgy brake pads that used for C/C-SiC disc, Tribol. Int. 154 (2021), 106686, https://doi.org/10.1016/j.triboint.2020.106686.

[19] X. Li, Disc identification and wear trend prediction based on support vector machine and least squares support vector machine, Railw. Qual. Contr. 46 (10) (2018) 29–32+38, https://doi.org/10.3969/j.issn.1006-9178.2018.10.010.

[20] S. Kumar, Priyadarshan, S.K. Ghosh, Statistical and artificial neural network technique for prediction of performance in AlSi10Mg-MWCNT based composite materials, Mater. Chem. Phys. 273 (2021), 125136, https://doi.org/10.1016/j.matchemphys.2021.125136.

[21] M. Wang, H.L. Wang, J.P. Wang, Wear volume prediction of brake shoes used in heavy freight wagon based on DBN, Comput. Simulat. 39 (2022) 134–139, https://doi.org/10.3969/j.issn.1006-9348.2022.03.026, 03.

[22] W.X. Xu, M. Zhang, J.L. Mo, R.H. Hu, Monitoring of partial wear state of brake sluice friction block of high speed train based on CBAM-CNN. Tribology. 1–16. https://doi.org/10.16078/j.tribology.2021264.

[23] X.G. Zhu, L.M. Sun, Y. Chen, Y.Z. Zhang, Tribological performances of cu-based powder metallurgy brake pads under high-speed braking condition, Lubric. Eng. 40 (11) (2015) 52–55+59, https://doi.org/10.3969/j.issn.0254-0150.2015.11.010.

[24] J.F. Li, D. Lu, H.X. Li, An improved atomic search algorithm, J. Syst. Simul. 34 (2022) 490–502, https://doi.org/10.16182/j.issn1004731x.joss.20-0824, 03.

[25] Y.Y. Luo, Y.P. Wang, Z.H. Sun, H. Liang, Study on ultrasonic recognition and performance degradation model of electrical connector fretting wear. China Mechanical Engineering. 1-9. http://kns.cnki.net/kcms/detail/42.1294.th.20220424.1446.008.html.

[26] Y.Q. Huang, D.X. Chi, L.L. Xu, Research on few-shot learning based on embedding learning, Comput. Eng. Appl. 58 (2022) 34–49, https://doi.org/10.3778/j.issn.1002-8331.2108-0213, 03.